Journal of Materials Chemistry A

PAPER

View Article Online
View Journal

Cite this: DOI: 10.1039/c5ta02502h

A dopant-free organic hole transport material for efficient planar heterojunction perovskite solar cells†

Yongsheng Liu,[ab] Qi Chen,[ab] Hsin-Sheng Duan,[ab] Huanping Zhou,[ab] Yang (Michael) Yang,[a] Huajun Chen,[a] Song Luo,[ab] Tze-Bin Song,[ab] Letian Dou,[ab] Ziruo Hong[a] and Yang Yang*[ab]

Received 7th April 2015
Accepted 23rd April 2015

DOI: 10.1039/c5ta02502h

www.rsc.org/MaterialsA

We demonstrate efficient planar perovskite solar cells using a dopant-free donor–acceptor (D–A) conjugated small molecule as a hole transport material. The photovoltaic cell reaches a power conversion efficiency (PCE) of 14.9%, which is comparable to or even better than that of the devices using the traditional doped 2,2′,7,7′-tetrakis(*N*,*N*′-di-*p*-methoxyphenylamine)-9,9′-spirobifluorene (spiro-OMeTAD) hole transport material under equivalent conditions. We ascribe the high performance to the excellent charge transporting properties of the D–A conjugated small molecule. Time-resolved photoluminescence (PL), transient photocurrent response, and impedance spectroscopy characterization indicate that this D–A conjugated small molecule plays a key role in hole collection and extraction in perovskite based photovoltaic devices. The dopant-free D–A small molecule hole transport material used here not only improves the efficiency, but also facilitates the fabrication process and thus potentially reduces the fabrication cost of perovskite solar cells.

Introduction

Photovoltaic technology is one of the most effective approaches to utilize solar energy, which directly converts sunlight into electricity. Presently, the majority of commercial solar cells are based on inorganic materials such as silicon.[1] However, the high cost and large energy consumption of raw materials and expensive fabrication processes of the solar cells hinder their wide applications. To produce low-cost and high efficiency solar cells, many new photovoltaic technologies are being developed,[2–6] which include perovskite based organic–inorganic hybrid solar cells. This new class of photovoltaic devices has the promise to compete with current commercialized inorganic solar cells as they feature both a low cost fabrication process as well as high efficiency.

Recently, hybrid metal halide perovskites such as $CH_3NH_3PbI_3$ and $CH_3NH_3PbI_{3-x}Cl_x$ showed high photovoltaic performance due to their direct band gap, large absorption coefficient and high charge carrier mobility as well as very low loss in charge recombination.[7–12] A previously reported power conversion efficiency (PCE) of 3.8% in 2009 has been increased to over 16%, as new materials and novel device protocols were developed in the past few years.[8–11,13–21] Although perovskites are efficient light harvesting materials with bipolar transport properties, recent reports of hole transport layer (HTL) free $TiO_2/CH_3NH_3PbI_3$ heterojunction solar cells have resulted in PCEs of 8–10.85%,[22,23] which are still much lower than those of the devices with HTLs. It indicates the necessity of interface modification for effective hole extraction from the perovskite layer to the anode. An appropriate energy level alignment and good hole transport properties should be guaranteed to minimize any loss in electrical potential and charge recombination. To date, some HTL materials have been demonstrated in high-performance hybrid solar cells, among which 2,2′,7,7′-tetrakis(*N*,*N*′-di-*p*-methoxyphenylamine)-9,9′-spirobifluorene (spiro-OMeTAD) is the ubiquitous material used. Using spiro-OMeTAD as a HTL, a PCE of over 15% has been reported.[15,16,20,21]

Spiro-OMeTAD HTL based perovskite photovoltaic devices have achieved the highest PCEs so far.[21] However, a pristine spiro-OMeTAD film suffers from a low hole mobility of $\sim 10^{-4}$ $cm^2\ V^{-1}\ s^{-1}$ and a low conductivity of $\sim 10^{-5}$ S cm^{-2} (compared with 10^{-3} S cm^{-1} for a typical halide perovskite) due to its amorphous nature.[24,25] Thus ionic additives or p-type dopants, such as lithium bis(trifluoromethylsulfonyl)-imide (Li-TFSI), are required for a spiro-OMeTAD HTL to generate free carriers and to increase its conductivity.[8,13,16] However, this material still has several disadvantages such as: (1) material cost due to the necessity of a thick spiro-OMeTAD layer (typically ~300

[a]Department of Materials Science and Engineering, University of California, Los Angeles, California 90095, USA. E-mail: yangy@ucla.edu

[b]California NanoSystems Institute, University of California, Los Angeles, California 90095, USA

† Electronic supplementary information (ESI) available: Additional spectroscopic and *J*–*V* data, information about the organic field-effect transistors, XRD and AFM, and the box chart of device parameters. See DOI: 10.1039/c5ta02502h

nm);[16,20,21] (2) degradation of perovskite active layer as spiro-OMeTAD HTL based devices require exposure to ambient atmosphere for proper functioning;[26,27] and (3) complex fabrication due to the spiro-OMeTAD doping process.[28]

Thus alternative hole transport materials should be developed to replace spiro-OMeTAD.[29–39] Recently, a doped low band gap polymer, PDPPDBTE, was incorporated as a HTL by Park *et al.* and the devices showed a PCE of 9.2%.[34] Seok *et al.* introduced a doped polymer hole transport material, poly-(triarylamine) (PTAA), yielding a certified PCE of 17.9% very recently, making PTAA the best polymer HTL so far.[37] In addition, several conjugated polymers, such as P3HT, PCPDTBT and PCDTBT and so on, can be used, in spite of their inferior PCEs.[29,32] In all the cases, the doping process is necessary, indicating that these materials cannot afford enough carrier mobility, and thus certain carrier concentration is required for efficient hole extraction from the perovskite film. These potential challenges for HTLs, including their high cost, low mobility, and requirement of doping, should be tackled in order for us to make further advancement of perovskite solar cells.

As discussed above, an dopant-free HTL is highly desirable, though there has been no report on excellent photovoltaic performance based on HTL materials with such properties. Donor–Acceptor (D–A) conjugated small molecules with planar structures have tunable optical and electrical properties, facile synthesis procedures, low production cost, and versatile wet processing procedures. The strong intermolecular interaction makes strong crystallization in solid thin films, and enables high charge carrier mobility. Therefore D–A conjugated small molecules are appropriate choices as HTLs and have been widely used as active semiconductor materials in organic electronic devices. Conjugated D–A small molecule HTLs having a planar structure without a diphenylamine group, which is a component of spiro-OMeTAD, increase the crystallinity and improve the mobility and conductivity of the pristine film. Also these molecules have an easily tunable HOMO (highest occupied molecular orbital) energy level to allow for an appropriate alignment with the perovskite absorbers. Thus D–A conjugated small molecule HTLs, though few, have shown good performance for perovskite solar cells.[40,41] However, the study and comparison of D–A conjugated small molecules and traditional spiro-OMeTAD HTLs' effect on the performance of perovskite solar cells have rarely been reported.[42,43]

In this work, we introduced a D–A conjugated small molecule DOR3T-TBDT (Fig. 1), which showed good performance as a donor material in organic solar cells,[44] as a dopant-free HTL in organic–inorganic hybrid solar cells consisting of $CH_3NH_3PbI_{3-X}Cl_X$ as the light harvester and TiO_2 as the electron transport layer (ETL). The photovoltaic devices using doped or dopant-free spiro-OMeTAD HTLs were also fabricated and tested for comparison. The device structure is ITO/TiO_2/$CH_3NH_3PbI_{3-X}Cl_X$/HTL/MoO_3/Ag. The optimized devices showed a PCE of up to 14.9%, which is the highest reported value so far for perovskite solar cells using a dopant-free HTL. The performance of the perovskite solar cells using a dopant-free small molecule HTL is comparable to or even better than that of the devices using a traditional doped spiro-OMeTAD HTL under equivalent conditions. Our results highlight the application promise of the organic–inorganic hybrid perovskite solar cells using D–A conjugated small molecules with a planar structure as a dopant-free HTL due to their good packing structures and thus relatively high mobility and conductivity.

Results and discussion

The resistivity of DOR3T-TBDT was measured by a transmission line model at room temperature, showing a bulk conductivity of $\sim 4 \times 10^{-4}$ S cm^{-1}, which is comparable with those of lead halide perovskite ($\sim 10^{-3}$ S cm^{-1}) and doped spiro-OMeTAD ($\sim 10^{-4}$ S cm^{-1}).[45] High conductivity is expected to reduce the series resistance and improve the FF. The high conductivity is partially due to the high hole mobility. By using DOR3T-TBDT as a semiconductor layer in a standard bottom-contact organic field-effect transistor (OFET), the hole mobility of DOR3T-TBDT extracted from the linear regime was 0.26 cm^2 V^{-1} s^{-1}, which is three orders of magnitude larger than that of pristine spiro-OMeTAD ($\sim 10^{-4}$ cm^2 V^{-1} s^{-1}).[25]

The cross-sectional SEM image and schematic of the device structure are shown in Fig. 1b and c. The overlayer of the small molecule HTL is seen to uniformly cap the perovskite layer. The cross-sectional SEM image of the device confirms that the device configuration is a well-defined layer-by-layer structure. The thicknesses of the TiO_2, $CH_3NH_3PbI_{3-X}Cl_X$ and DOR3T-TBDT layers are ~40, ~320, and ~60 nm, respectively. Here, the $CH_3NH_3PbI_{3-X}Cl_X$ layer is thick enough to serve as the light absorber and can effectively extract the charge carrier due to its long carrier diffusion lengths and good charge transport properties.[46] Fig. 1d shows the relevant energy level diagram of the materials used to prepare the perovskite solar cells. In the case of $CH_3NH_3PbI_{3-X}Cl_X$, the valance band (VB) is ~5.4 eV, which is measured using ultraviolet photoelectron spectroscopy (UPS).[47] Note that the HOMO level of DOR3T-TBDT is −5.5 eV according to cyclic voltammetry (CV) measurements in its film state.[44] For comparison, we measured the HOMO level of DOR3T-TBDT and spiro-OMeTAD in film states using UPS (Fig. S2, ESI†). The HOMO levels of DOR3T-TBDT and spiro-OMeTAD are calculated to be −5.1 and −5.0 eV, respectively. The LUMO level of −3.3 eV for DOR3T-TBDT was calculated from its optical band gap (1.77 eV)[42] and HOMO level. As can be seen by the band alignment, $CH_3NH_3PbI_{3-X}Cl_X$ has a matched band position for heterojunction solar cells with TiO_2 as the ETL and DOR3T-TBDT as the HTL.

The top-view scanning electron microscopy (SEM) images of the $CH_3NH_3PbI_{3-X}Cl_X$ film on TiO_2 and the DOR3T-TBDT film on $CH_3NH_3PbI_{3-X}Cl_X$ are shown in Fig. 1e and f. The results reveal that the perovskite film is uniform but exhibits relatively high roughness, though after coating the small molecule HTL on the top of the perovskite layer, the surface appears smooth with complete coverage by the HTL. The thin layer of DOR3T-TBDT efficiently prevents direct contact between the $CH_3NH_3PbI_{3-X}Cl_X$ layer and the electrode, and at the same time plays a role in both hole extraction and transport. The surface morphology can also be seen from the tapping mode AFM images (5 μm × 5 μm) (insets of Fig. 1e and f). The roughness

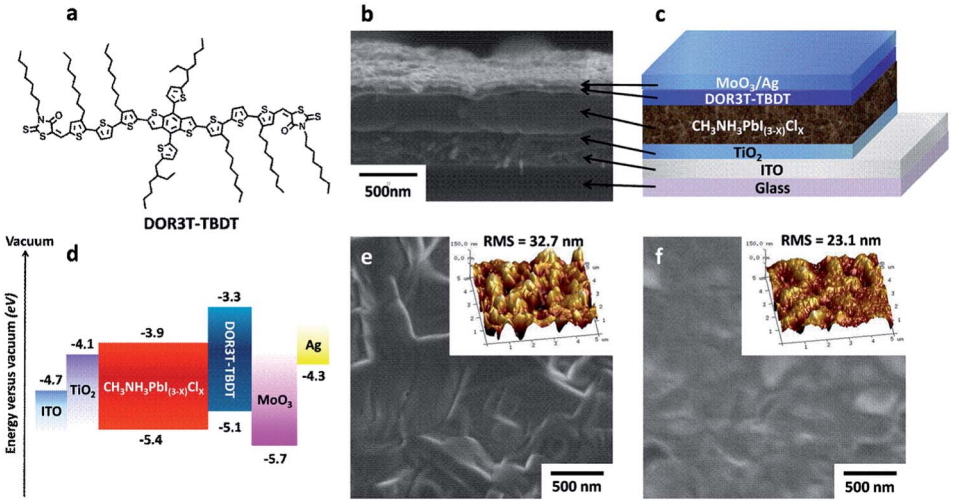

Fig. 1 (a) Chemical structure of the hole transport material DOR3T-TBDT. (b) SEM image of cross-sectional structure of the representative device. (c) Device structure of the solar cell. (d) Energy level diagram of the corresponding materials used in the device. (e) Top-view SEM images of glass/TiO_2/perovskite film; (f) top-view SEM images of glass/TiO_2/perovskite/DOR3T-TBDT film. Insets are the tapping-mode AFM 3D topographic images of the related films.

was reduced to 23.1 nm from 32.7 nm after spin coating a layer of DOR3T-TBDT on perovskite.

To understand the effect of HTL on the performance of perovskite solar cells, various HTL materials including dopant-free small molecule DOR3T-TBDT, and dopant-free and doped spiro-OMeTAD were used for comparison. Fig. 2a shows the current density–voltage (*J*–*V*) curves of the optimized performance of three types of devices. As can be seen in the *J*–*V* curves and the summarized performance parameters in Table 1, the device with dopant-free spiro-OMeTAD has a PCE of 3.5% with a low J_{SC} of 16.6 mA cm^{-2} and a poor FF of 22%. By reducing the incident light intensity to below 10 mW cm^{-2}, the FF increases to over 60% (Fig. S7, ESI†). It indicates that the low hole mobility and conductivity of dopant-free spiro-OMeTAD cause strong hole accumulation and the unusual *J*–*V* curve under AM1.5G 1 sun illumination. Using a doped spiro-OMeTAD HTL, we observed a dramatically enhanced performance with the highest PCE of 14.0%, combined with a J_{SC} of 19.5 mA cm^{-2}, an open circuit voltage (V_{OC}) of 1.04 V, and an FF of 69.0%, mainly due to the improved conductivity of the spiro-OMeTAD HTL,

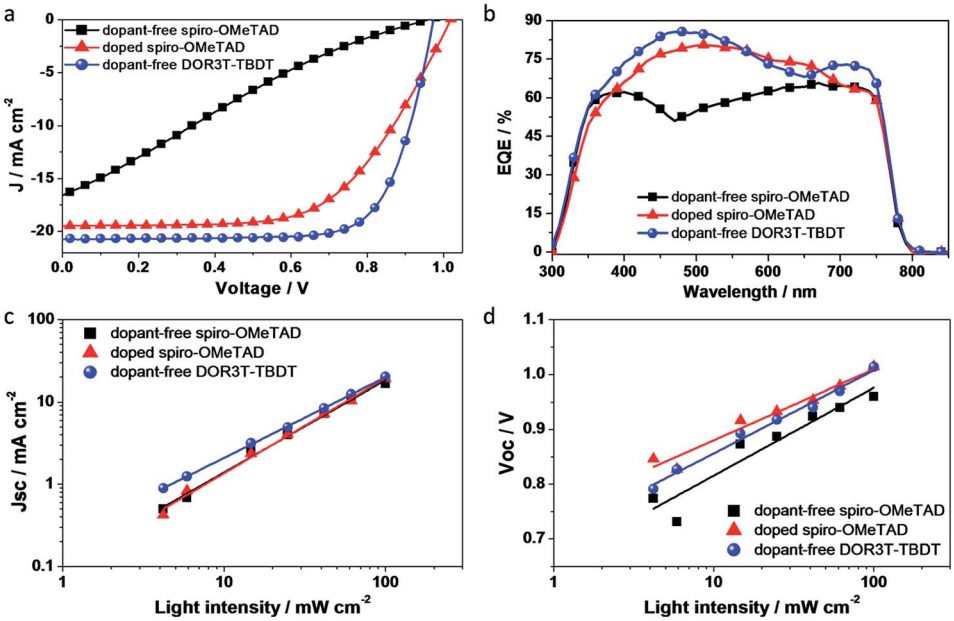

Fig. 2 (a) Current density *versus* voltage (*J*–*V*) curves of perovskite solar cells using different HTLs under AM 1.5 G irradiation at 100 mW cm^{-2}. (b) EQE of the corresponding device using different HTLs. (c) J_{SC} as a function of light intensity in a double logarithmic scale for devices using different HTLs. (d) V_{OC} as a function of light intensity in a semi-logarithmic scale for devices using different HTLs.

Table 1 Performance parameters for optimized photovoltaic devices prepared with different HTLs at reverse voltage scan

HTLs	V_{OC} (V)	J_{SC} (mA cm^{-2})	PCE (%)	FF (%)
Dopant-free spiro-OMeTAD	0.96	16.6	3.5	22
Doped spiro-OMeTAD	1.04	19.5	14.0	69
Dopant-free DOR3T-TBDT	0.97	20.7	14.9	74

which is consistent with previously published results.[46,48] Using DOR3T-TBDT as a HTL, the champion device exhibits a J_{SC} of 20.7 mA cm^{-2}, a V_{OC} of 0.97 V, and a very notable FF of 74%, yielding a PCE of 14.9%, which, to the best of our knowledge, is the highest PCE in planar heterojunction perovskite solar cells using an dopant-free HTL. The statistical data of perovskite solar cells containing dopant-free spiro-OMeTAD, doped spiro-OMeTAD and dopant-free DOR3T-TBDT HTLs are shown in Fig. S9 (ESI†). It is worth noting that the dopant-free DOR3T-TBDT HTL facilitates very good charge injection under the forward bias, and thus yields a very low series resistance. However the doped spiro-OMeTAD based device still exhibits higher resistance, which shall be responsible for the lower FF and slightly higher V_{OC} than those of DOR3T-TBDT based devices. Indeed, the overall performance of the device using a dopant-free DOR3T-TBDT HTL was comparable and even higher than that of the device using a doped spiro-OMeTAD HTL. The high performance may stem from the matched HOMO energy level, high mobility and conductivity of this small molecule. We further doped DOR3T-TBDT with the same dopants as in a spiro-OMeTAD HTL, however, the device showed a lower PCE (<10%) (Fig. S8, ESI†). Considering the doping efficiency, DOR3T-TBDT has a HOMO level of 5.1 eV, deeper than that of spiro-OMeTAD (5.0 eV). That means the dopants that work well with spiro-OMeTAD might not be able to generate free carriers in DOR3T-TBDT.[49] And also the dopants might play a negative role of disturbing the molecular packing. Nevertheless, p-type dopants with higher electron-affinity are expected to promote hole transport in the case of DOR3T-TBDT.

From the *J–V* curve in Fig. 2, the optimized device based on a dopant-free small molecule HTL shows a low serial resistance and good charge injection, resulting in a FF of 74%. The results indicate that this dopant-free small molecule HTL helps to form ohmic contact between perovskite and the anode for hole extraction and injection. Note that the film thickness of the DOR3T-TBDT HTL is ~60 nm, which is thinner than that (~300 nm) of the doped spiro-OMeTAD HTL. The thin DOR3T-TBDT layer can potentially reduce material consumption for mass production. Our results indicate that comparable or even higher performance can be obtained for perovskite solar cells using a dopant-free D–A small molecule with a planar structure as a HTL than that of dopant-free/doped spiro-OMeTAD HTLs (see ESI, Fig. S9,† for statistical analysis). Note that MoO_3 used here formed a high work function contact buffer for efficient hole injection/extraction, and protected the underneath layers from damage caused by Ag deposition.[50,51] Fig. 2b shows the EQE spectra of the devices using different HTLs and J_{SC} values calculated from the integral of EQE curves over AM1.5G solar spectrum are summarized in Table S1.† The perovskite solar cells using DOR3T-TBDT as the HTL show an excellent photocurrent response from 400 to 800 nm, with the EQE reaching a maximum of 86% at 480 nm, while dopant-free and doped spiro-OMeTAD based devices showed a maximum EQE of 66% at 670 nm and 80% at 510 nm, respectively. The EQE values indicate that the photoresponse is very efficient for the device using the DOR3T-TBDT HTL, which is slightly better than that of the doped spiro-OMeTAD HTL.

In order to further understand losses due to the carrier recombination in the device, light intensity dependence of *J–V* characteristics of the device using different HTLs was measured under illumination of a solar simulator with a set of neutral density filters. Shown in Fig. 2c is the linear relationship of the photocurrent with light intensity in a double logarithmic scale for the device using dopant-free/doped spiro-OMeTAD and DOR3T-TBDT with a slope of very close to 1, indicating that the bimolecular recombination is very weak in these devices. Fig. 2d gives V_{OC} as a function of light intensity. We can see that V_{OC} increases monotonically with light intensity for the perovskite solar cells using different HTLs. The dependence of V_{OC} on light intensity implies that trap-assisted Schockley-Read-Hall recombination plays a role.[52] We noticed that the slopes of V_{OC} *vs.* light intensity of the two high performance devices are still different. The doped spiro-OMeTAD based device has a smaller slope, which is tentatively ascribed to large shunt, since the thick HTL of 300 nm should be enough to ensure a large device shunt, and avoid any contact between the perovskite photoactive layer and the anode. On the other hand, the thickness of the dopant-free DOR3T-TBDT layer is much smaller (~60 nm). Though it forms full coverage over the perovskite layer as shown in Fig. 1b, the shunt may still play a role reducing the V_{OC} under weak light. Such recombination behaviors are consistent with FF *vs.* light intensity as shown in Fig. S7 (ESI†). The devices using dopant-free/doped spiro-OMeTAD showed a low FF with increasing light intensity, suggesting that charge recombination is dependent on the photogenerated carrier density. On the contrary, the device using the DOR3T-TBDT HTL showed a high FF nearly constant under variable light intensity.

So far we have shown that hole extraction and transport are strongly dependent on the HTLs. To further look into the charge dynamics, we measured charge generation of the perovskite films *via* steady-state photoluminescence (PL) and time-resolved PL characterization. The steady-state PL spectra of glass/$CH_3NH_3PbI_{3-X}Cl_X$, glass/TiO_2/$CH_3NH_3PbI_{3-X}Cl_X$, glass/$CH_3NH_3PbI_{3-X}Cl_X$/DOR3T-TBDT, and glass/TiO_2/$CH_3NH_3PbI_{3-X}Cl_X$/DOR3T-TBDT are shown in Fig. 3a. From the PL spectra, we observed a significant PL quenching when the perovskite layer is in contact with TiO_2 or the DOR3T-TBDT layer, indicating efficient charge transfer at both interfaces.[53,54] Compared with a perovskite film on the glass substrate structure, the PL intensity is quenched to ~0.5% for the perovskite layer coated on the glass/TiO_2 substrate. The DOR3T-TBDT coated perovskite film shows almost completely quenched PL, and the sample exhibits roughly 0.2% PL, suggesting that this dopant-free DOR3T-TBDT HTL can extract charge charier efficiently.

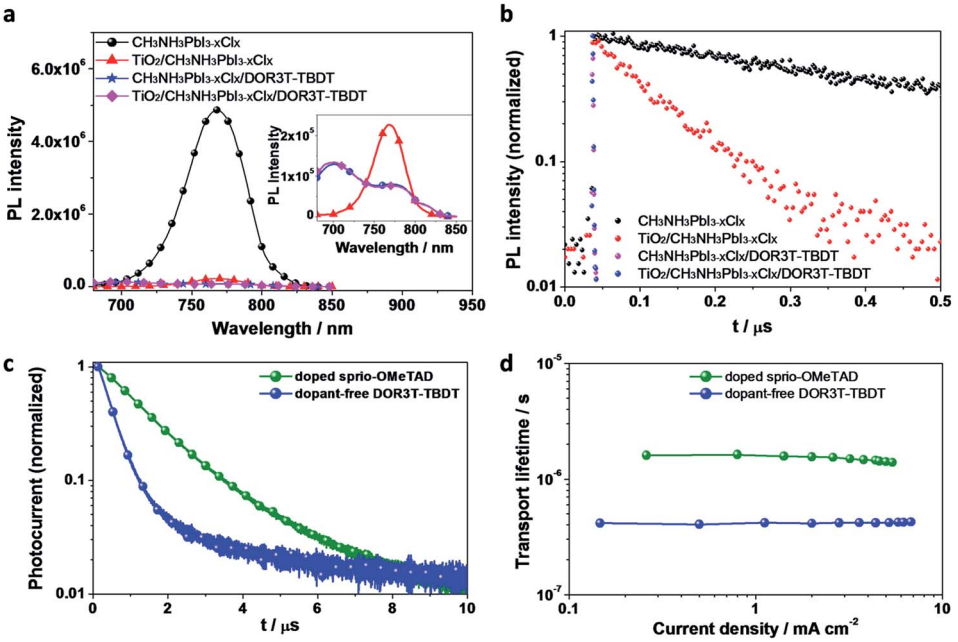

Fig. 3 (a) The steady-state PL spectra and (b) time-resolved PL decay transient spectra of glass/$CH_3NH_3PbI_{3-X}Cl_X$, glass/TiO_2/$CH_3NH_3PbI_{3-X}Cl_X$, glass/$CH_3NH_3PbI_{3-X}Cl_X$/DOR3T-TBDT, and glass/TiO_2/$CH_3NH_3PbI_{3-X}Cl_X$/DOR3T-TBDT. (c) Normalized photocurrent transients for perovskite solar cells with doped spiro-OMeTAD and dopant-free DOR3T-TBDT as the HTL, set to the same background illumination intensity (50 mW cm^{-2}). (d) Charge transport lifetime determined by small-perturbation transient photocurrent decay measurements of perovskite solar cells with doped spiro-OMeTAD and dopant-free DOR3T-TBDT as HTLs.

The time-resolved PL decay has been measured *via* monitoring the peak emission at 768 nm as shown in Fig. 3b. Fitting the data with two-component exponential decay (here, the longer lifetime was used for comparison) yields the lifetime of carriers. The PL decay of the neat $CH_3NH_3PbI_{3-X}Cl_X$ film exhibits a PL lifetime of 483 ns, which is larger than previous reports,[46,53] and is tentatively ascribed to the Cl doping effect.[46] The PL lifetimes were substantially shortened when perovskite was interfaced with the TiO_2 layer with a PL lifetime of 80 ns. As shown in Fig. 3b, the decay of the perovskite/DOR3T-TBDT is significantly faster than that of TiO_2/perovskite. In addition, the PL lifetime cannot be monitored at the current temporal resolution, which indicates efficient charge-carrier transfer at the perovskite/DOR3T-TBDT interface.

To further investigate the dynamical processes operating under real device conditions, we measured the carrier lifetimes by transient photocurrent measurements. As shown in Fig. 3c, we observed that the DOR3T-TBDT devices exhibit faster transient photocurrent decays as compared to doped spiro-OMeTAD devices over various background light bias. Fig. 3d displays the normalized photocurrent transients for DOR3T-TBDT based cells and for doped spiro-OMeTAD based cells, showing that the carrier collection in DOR3T-TBDT based cells is enhanced. Our results indicate that hole extraction has been improved by replacing doped spiro-OMeTAD with DOR3T-TBDT.

Again carrier recombination is still one of the major loss channels in photovoltaic cells. To gain more insight into the issue, electrochemical impedance spectroscopy (EIS) measurements were conducted on the completed devices under working conditions. Representative impedance spectra of perovskite devices using doped spiro-OMeTAD, dopant-free spiro-OMeTAD or DOR3T-TBDT as the HTL were recorded at different applied voltages over the frequency range of 100 Hz to 1 MHz under simulated AM1.5G 1 sun illumination (100 mW cm^{-2}). As shown in Fig. 4, the Nyquist plots of these devices show two distinct features: (1) one main arc is observed for all the devices over the frequency range in the measurement; (2) a second arc can be partially seen in the spectra of the doped spiro-OMeTAD and DOR3T-TBDT cells. The absence of transmission line behavior, which is usually associated with significant tail states of TiO_2, is likely due to the very thin TiO_2 layer employed in the devices.[30] For mesoporous TiO_2 based solid state dye sensitized solar cells, the high frequency features represent the hole transport properties.[55–57] In addition, since the active layer and ETL conditions are kept the same, the different diameters (resistance) shall be related to the carrier transport and contact-resistance in various HTL layers. Thus, we fitted the spectra with a resistance in series of a high frequency parallel RC circuit, so as to extract the information regarding hole transport and extraction. We exclude the low frequency features in the fitting, considering that the electron transport is not in the scope of this study. The fitting results are summarized in Fig. 4d, showing the dependence of the hole transport resistance on applied voltages. The hole transport resistance decreases with the increasing potential for both DOR3T-TBDT and doped spiro-OMeTAD based devices, and the resistance value for the DOR3T-TBDT based device decreases more dramatically than that of doped spiro-OMeTAD, indicating the smoother carrier movement as a result of reduced resistive losses. This is consistent with its enhanced FF. In contrast, the device using a

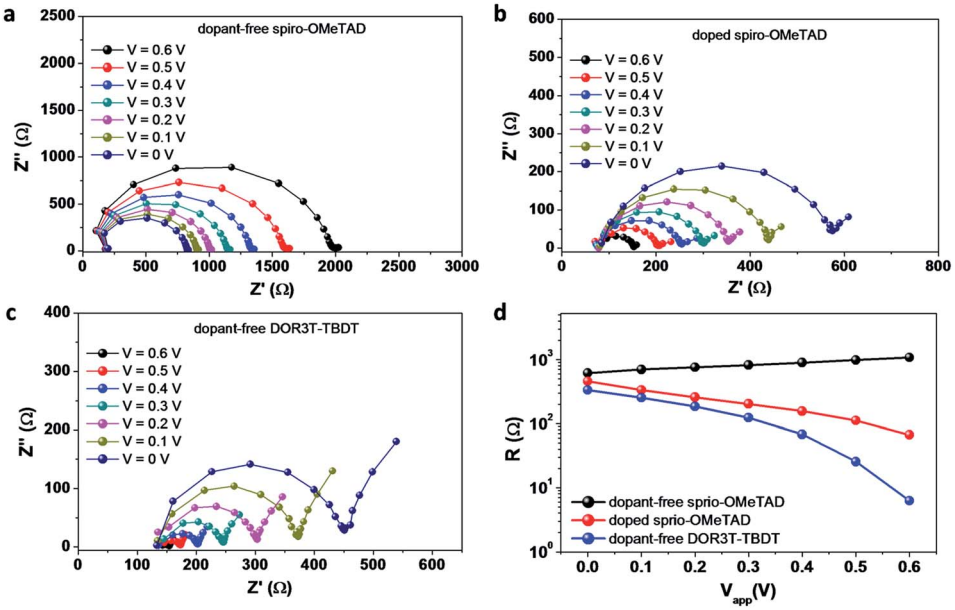

Fig. 4 Bias dependence of Cole–Cole plots of the device with (a) dopant-free spiro-OMeTAD HTL (b) doped spiro-OMeTAD HTL (c) dopant-free DOR3T-TBDT HTL. (d) Resistance extracted from impedance spectroscopy measurements at different potentials.

dopant-free spiro-OMeTAD HTL exhibits severe charge accumulation due to poor hole conductivity in the HTL, and the behavior of the solar cell resembles that of a huge resistor or injection barrier due to the lack of doping ions in spiro-OMeTAD. It might be a concern that the absorption of the HTL overlaps with that of the perovskite photoactive layer, and reduces the photovoltaic efficiency. We argue that the photogenerated excitons can still be converted into free carriers and collected with a suitable device design.[58] Note that the representative perovskite/DOR3T-TBDT based device shows hysteresis in the *J–V* curves (Fig. S10, ESI†), which is similar to those seen in typical perovskite devices.[21,59–61] The detailed data are shown in Table S2 (ESI†).

Conclusions

In conclusion, we have successfully demonstrated efficient planar structure perovskite solar cells employing a dopant-free small molecule HTL. The optimized device exhibits an impressive PCE of 14.9%, which is comparable to or even better than that of the devices using a traditional doped spiro-OMeTAD hole transport layer under equivalent conditions, and thus highlights the potential of a dopant-free small molecule HTL for high performance perovskite solar cells. Time-resolved photoluminescence (PL), transient photocurrent, and impedance spectra characterization indicate that this D–A conjugated small molecule can efficiently extract holes from the perovskite film to the anode. Our device legitimizes the use of D–A small molecules as HTLs in perovskite based solar cells as our small molecule HTL improves the efficiency, facilitates the fabrication process and reduces the fabrication cost. Our results indicate that D–A conjugated small molecules, which have a good packing structure and thus relatively high mobility and conductivity, are a class of promising hole transporting materials, and thus broader organic molecular semiconductors can be applied to perovskite solar cells. The use of dopant-free D–A conjugated small molecule HTLs will greatly enhance the potential for commercial applications of perovskite solar cells and thus can compete with the traditional inorganic solar cells.

Experimental section

Solar cell fabrication and measurements

A 40 nm-thick layer of a TiO_2 nanoparticle in ethanol with the appropriate amount of TiAcAc was spin-coated onto an ITO glass substrate and annealed at 150 °C for 30 min. Next, the substrates were transferred into a nitrogen-filled glove box. A solution of $CH_3NH_3PbI_{3-X}Cl_X$ in DMF was then spin coated onto the ITO/TiO_2 substrate by spin-coating at 2000 rpm for 30 s. For the $CH_3NH_3PbI_{3-X}Cl_X$ perovskite layer, the CH_3NH_3I powder was mixed with $PbCl_2$ at a 3 : 1 mol ratio in DMF at 60 °C for 12 h. Specifically, the concentration of the $PbCl_2$ and CH_3NH_3I was 0.7 and 2.1 M, respectively. The films were then dried on a hot plate at 95 °C for 90 min in air. The dopant-free DOR3T-TBDT HTL was spin-coated onto the perovskite layer. Here the concentration of DOR3T-TBDT is 18 mg mL^{-1} in chloroform and the film thickness is ~60 nm. The doped DOR3T-TBDT/chloroform (18 mg mL^{-1}, 0.4 mL) solution was prepared with the addition of 3 μL Li-TFSI/acetonitrile (260 mg mL^{-1}), and 5 μL *tert*-butylpyridine (tBP). The doped or dopant-free spiro-OMeTAD HTL was coated by spin coating (2000 r.p.m. for 30 s) 25 μL of chlorobenzene solution. The spiro-OMeTAD without the dopant has the concentration of 160 mg mL^{-1}. For a doped solution, a spiro-OMeTAD/chlorobenzene (160 mg/1 mL) solution was employed with the addition of 35 μL Li-TFSI/acetonitrile (260 mg mL^{-1}), and 28 μL 4-*tert*-Butylpyridine. Finally, a 15 nm MoO_3 layer and a

150 nm Ag layer were deposited in sequence on the HTL through shadow masks *via* thermal evaporation under high vacuum ($\sim 2 \times 10^{-6}$ Torr). The effective area was 0.1 cm^2. The current density–voltage (*J–V*) characteristics of photovoltaic devices were obtained using a Keithley 2400 source-measure unit. The photocurrent was measured under AM 1.5 G illumination at 100 mW cm^{-2} under a Newport Thermal Oriel 91192 1000 W solar simulator. Unless stated otherwise, the devices were masked and measured under the reverse voltage scan with a scan rate of 1 V s^{-1}. The light intensity was calibrated using a KG-5 Si diode. External quantum efficiencies were measured by an Enli Technology (Taiwan) EQE measurement system. The effective area of each cell was 0.1 cm^2 defined by masks for all the photovoltaic devices discussed in this work.

Transient photocurrent decay measurements

A white light bias was generated from an array of diodes (Molex 180081-4320) to simulate 1 sun working conditions. A pulsed red dye laser (Rhodamine 6G, 590 nm) pumped using a nitrogen laser (LSI VSL-337ND-S) was used as the perturbation source, with a pulse width of 4 ns and a repetition frequency of 10 Hz. The perturbation light intensity was attenuated to keep the amplitude of transient ΔV below 5 mV. The current dynamics were recorded on a digital oscilloscope (Tektronix DPO 4104B), and the currents under short circuit conditions were measured over a 50 Ω resistor.

Impedance spectroscopy measurements

The complex impedance of the devices was recorded over the frequency range of 100 Hz to 1 MHz at room temperature under 1 sun, using the Z-θ mode of a HP 4284A LCR precision meter. An AC drive bias of 30 mV and different DC voltages range from 0 to 0.9 V with a step of 0.1 V was employed. The EIS Spectrum Analyzer was used for the fitting of the impedance spectra.

Acknowledgements

The authors gratefully acknowledge the financial support from the Office of Naval Research (Grant no. N000141110250), National Science Foundation (Grant no. DMR-1335645), and the Enli Tech (in Taiwan) for donating the EQE measurement system to UCLA. The authors would like to thank Dr. Jingbi You and Dr. Wan-Ching Hsu for helpful discussion and Mr. Eric Young and Mr. Nicholas De Marco for proofreading this manuscript. The authors would finally like to thank and acknowledge the use of the Nano and Pico Characterization Lab at the California NanoSystems Institute for AFM analysis.

References

1 T. Saga, *NPG Asia Mater.*, 2010, **2**, 96–102.
2 M. A. Green, K. Emery, Y. Hishikawa, W. Warta and E. D. Dunlop, *Prog. Photovoltaics*, 2014, **22**, 1–9.
3 G. Li, R. Zhu and Y. Yang, *Nat. Photonics*, 2012, **6**, 153–161.
4 S. Mathew, A. Yella, P. Gao, R. Humphry-Baker, B. F. E. Curchod, N. Ashari-Astani, I. Tavernelli, U. Rothlisberger, M. K. Nazeeruddin and M. Gratzel, *Nat. Chem.*, 2014, **6**, 242–247.
5 R. F. Service, *Science*, 2013, **342**, 794–797.
6 N. G. Park, *J. Phys. Chem. Lett.*, 2013, **4**, 2423–2429.
7 C. C. Stoumpos, C. D. Malliakas and M. G. Kanatzidis, *Inorg. Chem.*, 2013, **52**, 9019–9038.
8 H. S. Kim, C. R. Lee, J. H. Im, K. B. Lee, T. Moehl, A. Marchioro, S. J. Moon, R. Humphry-Baker, J. H. Yum, J. E. Moser, M. Gratzel and N. G. Park, *Sci. Rep.*, 2012, **2**, 591.
9 P. Gao, M. Gratzel and M. K. Nazeeruddin, *Energy Environ. Sci.*, 2014, **7**, 2448–2463.
10 M. A. Green, A. Ho-Baillie and H. J. Snaith, *Nat. Photonics*, 2014, **8**, 506–514.
11 A. Kojima, K. Teshima, Y. Shirai and T. Miyasaka, *J. Am. Chem. Soc.*, 2009, **131**, 6050–6051.
12 M. Gratzel, *Nat. Mater.*, 2014, **13**, 838–842.
13 J. Burschka, N. Pellet, S. J. Moon, R. Humphry-Baker, P. Gao, M. K. Nazeeruddin and M. Gratzel, *Nature*, 2013, **499**, 316–319.
14 Q. Chen, H. P. Zhou, Z. R. Hong, S. Luo, H. S. Duan, H. H. Wang, Y. S. Liu, G. Li and Y. Yang, *J. Am. Chem. Soc.*, 2014, **136**, 622–625.
15 M. M. Lee, J. Teuscher, T. Miyasaka, T. N. Murakami and H. J. Snaith, *Science*, 2012, **338**, 643–647.
16 M. Z. Liu, M. B. Johnston and H. J. Snaith, *Nature*, 2013, **501**, 395–398.
17 J. B. You, Z. R. Hong, Y. Yang, Q. Chen, M. Cai, T. B. Song, C. C. Chen, S. R. Lu, Y. S. Liu, H. P. Zhou and Y. Yang, *ACS Nano*, 2014, **8**, 1674–1680.
18 N. J. Jeon, H. G. Lee, Y. C. Kim, J. Seo, J. H. Noh, J. Lee and S. I. Seok, *J. Am. Chem. Soc.*, 2014, **136**, 7837–7840.
19 N. J. Jeon, J. H. Noh, Y. C. Kim, W. S. Yang, S. Ryu and S. I. Seok, *Nat. Mater.*, 2014, **13**, 897–903.
20 J. W. Lee, D. J. Seo, A. N. Cho and N. G. Park, *Adv. Mater.*, 2014, **26**, 4991–4998.
21 H. P. Zhou, Q. Chen, G. Li, S. Luo, T. B. Song, H. S. Duan, Z. R. Hong, J. B. You, Y. S. Liu and Y. Yang, *Science*, 2014, **345**, 542–546.
22 W. Abu Laban and L. Etgar, *Energy Environ. Sci.*, 2013, **6**, 3249–3253.
23 S. Aharon, S. Gamliel, B. El Cohen and L. Etgar, *Phys. Chem. Chem. Phys.*, 2014, **16**, 10512–10518.
24 J. Burschka, A. Dualeh, F. Kessler, E. Baranoff, N. L. Cevey-Ha, C. Y. Yi, M. K. Nazeeruddin and M. Gratzel, *J. Am. Chem. Soc.*, 2011, **133**, 18042–18045.
25 T. Leijtens, I. K. Ding, T. Giovenzana, J. T. Bloking, M. D. McGehee and A. Sellinger, *ACS Nano*, 2012, **6**, 1455–1462.
26 A. Abate, T. Leijtens, S. Pathak, J. Teuscher, R. Avolio, M. E. Errico, J. Kirkpatrik, J. M. Ball, P. Docampo, I. McPherson and H. J. Snaith, *Phys. Chem. Chem. Phys.*, 2013, **15**, 2572–2579.
27 G. E. Eperon, V. M. Burlakov, P. Docampo, A. Goriely and H. J. Snaith, *Adv. Funct. Mater.*, 2014, **24**, 151–157.
28 J. Liu, Y. Z. Wu, C. J. Qin, X. D. Yang, T. Yasuda, A. Islam, K. Zhang, W. Q. Peng, W. Chen and L. Y. Han, *Energy Environ. Sci.*, 2014, **7**, 2963–2967.

29 D. Q. Bi, L. Yang, G. Boschloo, A. Hagfeldt and E. M. J. Johansson, *J. Phys. Chem. Lett.*, 2013, **4**, 1532–1536.
30 J. A. Christians, R. C. M. Fung and P. V. Kamat, *J. Am. Chem. Soc.*, 2014, **136**, 758–764.
31 B. Conings, L. Baeten, C. D. Dobbelaere, J. D'Haen, J. Manca and H. G. Boyen, *Adv. Mater.*, 2014, **26**, 2041–2046.
32 J. H. Heo, S. H. Im, J. H. Noh, T. N. Mandal, C. S. Lim, J. A. Chang, Y. H. Lee, H. J. Kim, A. Sarkar, M. K. Nazeeruddin, M. Gratzel and S. I. Seok, *Nat. Photonics*, 2013, **7**, 487–492.
33 A. Krishna, D. Sabba, H. R. Li, J. Yin, P. P. Boix, C. Soci, S. G. Mhaisalkar and A. C. Grimsdale, *Chem. Sci.*, 2014, **5**, 2702–2709.
34 Y. S. Kwon, J. Lim, H. J. Yun, Y. H. Kim and T. Park, *Energy Environ. Sci.*, 2014, **7**, 1454–1460.
35 O. Malinkiewicz, A. Yella, Y. H. Lee, G. M. Espallargas, M. Graetzel, M. K. Nazeeruddin and H. J. Bolink, *Nat. Photonics*, 2014, **8**, 128–132.
36 P. Qin, S. Tanaka, S. Ito, N. Tetreault, K. Manabe, H. Nishino, M. K. Nazeeruddin and M. Gratzel, *Nat. Commun.*, 2014, **5**, 3834.
37 N. J. Jeon, J. H. Noh, W. S. Yang, Y. C. Kim, S. C. Ryu, J. W. Seo and S. I. Seok, *Nature*, 2015, **517**, 476–480.
38 S. Guarnera, A. Abate, W. Zhang, J. M. Foster, G. Richardson, A. Petrozza and H. J. Snaith, *J. Phys. Chem. Lett.*, 2015, **6**, 432–437.
39 Z. Hawash, L. K. Ono, S. R. Raga, M. V. Lee and Y. B. Qi, *Chem. Mater.*, 2015, **27**, 562–569.
40 P. Qin, S. Paek, M. I. Dar, N. Pellet, J. Ko, M. Gratzel and M. K. Nazeeruddin, *J. Am. Chem. Soc.*, 2014, **136**, 8516–8519.
41 P. Qin, H. Kast, M. K. Nazeeruddin, S. M. Zakeeruddin, A. Mishra, P. Bauerle and M. Gratzel, *Energy Environ. Sci.*, 2014, **7**, 2981–2985.
42 M. Cheng, C. Chen, X. C. Yang, J. Huang, F. G. Zhang, B. Xu and L. C. Sun, *Chem. Mater.*, 2015, **27**, 1808–1814.
43 Y. K. Song, S. T. Lv, X. C. Liu, X. G. Li, S. R. Wang, H. Y. Wei, D. M. Li, Y. Xiao and Q. B. Meng, *Chem. Commun.*, 2014, **50**, 15239–15242.
44 Y. S. Liu, C. C. Chen, Z. R. Hong, J. Gao, Y. Yang, H. P. Zhou, L. T. Dou, G. Li and Y. Yang, *Sci. Rep.*, 2013, **3**, 3356.
45 T. Leijtens, J. Lim, J. Teuscher, T. Park and H. J. Snaith, *Adv. Mater.*, 2013, **25**, 3227–3233.
46 S. D. Stranks, G. E. Eperon, G. Grancini, C. Menelaou, M. J. P. Alcocer, T. Leijtens, L. M. Herz, A. Petrozza and H. J. Snaith, *Science*, 2013, **342**, 341–344.
47 P. Schulz, E. Edri, S. Kirmayer, G. Hodes, D. Cahen and A. Kahn, *Energy Environ. Sci.*, 2014, **7**, 1377–1381.
48 K. Wojciechowski, M. Saliba, T. Leijtens, A. Abate and H. J. Snaith, *Energy Environ. Sci.*, 2014, **7**, 1142–1147.
49 K. Walzer, B. Maennig, M. Pfeiffer and K. Leo, *Chem. Rev.*, 2007, **107**, 1233–1271.
50 D. W. Zhao, P. Liu, X. W. Sun, S. T. Tan, L. Ke and A. K. K. Kyaw, *Appl. Phys. Lett.*, 2009, **95**, 153304.
51 T. Hori, T. Shibata, V. Kittichungchit, H. Moritou, J. Sakai, H. Kubo, A. Fujii and M. Ozaki, *Thin Solid Films*, 2009, **518**, 522–525.
52 M. M. Mandoc, F. B. Kooistra, J. C. Hummelen, B. de Boer and P. W. M. Blom, *Appl. Phys. Lett.*, 2007, **91**, 263505.
53 G. C. Xing, N. Mathews, S. Y. Sun, S. S. Lim, Y. M. Lam, M. Gratzel, S. Mhaisalkar and T. C. Sum, *Science*, 2013, **342**, 344–347.
54 H. Najafov, B. Lee, Q. Zhou, L. C. Feldman and V. Podzorov, *Nat. Mater.*, 2010, **9**, 938–943.
55 H. S. Kim, J. W. Lee, N. Yantara, P. P. Boix, S. A. Kulkarni, S. Mhaisalkar, M. Gratzel and N. G. Park, *Nano Lett.*, 2013, **13**, 2412–2417.
56 A. Dualeh, T. Moehl, N. Tetreault, J. Teuscher, P. Gao, M. K. Nazeeruddin and M. Gratzel, *ACS Nano*, 2014, **8**, 362–373.
57 H. S. Kim, I. Mora-Sero, V. Gonzalez-Pedro, F. Fabregat-Santiago, E. J. Juarez-Perez, N. G. Park and J. Bisquert, *Nat. Commun.*, 2013, **4**, 2242.
58 Y. S. Liu, Z. R. Hong, Q. Chen, W. H. Chang, H. P. Zhou, T. B. Song, E. Young, Y. Yang, J. B. You, G. Li and Y. Yang, *Nano Lett.*, 2015, **15**, 662–668.
59 H. J. Snaith, A. Abate, J. M. Ball, G. E. Eperon, T. Leijtens, N. K. Noel, S. D. Stranks, J. T. W. Wang, K. Wojciechowski and W. Zhang, *J. Phys. Chem. Lett.*, 2014, **5**, 1511–1515.
60 E. L. Unger, E. T. Hoke, C. D. Bailie, W. H. Nguyen, A. R. Bowring, T. Heumuller, M. G. Christoforo and M. D. McGehee, *Energy Environ. Sci.*, 2014, **7**, 3690–3698.
61 H. S. Kim and N. G. Park, *J. Phys. Chem. Lett.*, 2014, **5**, 2927–2934.

